Enhanced orbital magnetic moment of Co film grown on Fe$_3$O$_4$(001)

Zhe Zhang ; Xianyang Lu ✉ ; Zhihao Li ; Zhuoyi Li ; Yu Yan; Yuzhe Chen; Jun Du ; Fangyuan Zhu; Jiefeng Cao; Yong Wang ; Yao Li ; Liang He ; Jing Wu ; Rong Zhang ; Yongbing Xu ✉

Check for updates

View Online   Export Citation

Articles You May Be Interested In

Direct observation of spin polarization in epitaxial Fe$_3$O$_4$(001)/MgO thin films grown by magnetron sputtering

Appl. Phys. Lett. (May 2022)

Interplay between magnetism and chemical structure at spinel-spinel interfaces

J. Appl. Phys. (May 2012)

Structural and magnetic properties of polycrystalline Fe$_3$O$_4$ thin film

AIP Conference Proceedings (May 2016)

Enhanced orbital magnetic moment of Co film grown on Fe₃O₄(001)

View Online   Export Citation   CrossMark

Zhe Zhang,[1] Xianyang Lu,[1,2,a] Zhihao Li,[1] Zhuoyi Li,[1] Yu Yan,[1] Yuzhe Chen,[1] Jun Du,[3] Fangyuan Zhu,[4] Jiefeng Cao,[4] Yong Wang,[4] Yao Li,[1] Liang He,[1] Jing Wu,[5] Rong Zhang,[1] and Yongbing Xu[1,2,5,a]

AFFILIATIONS

[1] Jiangsu Provincial Key Laboratory of Advanced Photonic and Electronic Materials, School of Electronic Science and Engineering, Nanjing University, Nanjing 210093, China
[2] School of Integrated Circuits, Nanjing University, Suzhou 215163, China
[3] Department of Physics, Nanjing University, Nanjing 210093, China
[4] Shanghai Synchrotron Radiation Facility, Shanghai Advanced Research Institute, Chinese Academy of Sciences, Shanghai 201204, China
[5] York-Nanjing International Joint Center in Spintronics, Department of Electronics and Physics, University of York, York YO10 5DD, United Kingdom

[a] Authors to whom correspondence should be addressed: xylu@nju.edu.cn and ybxu@nju.edu.cn

ABSTRACT

We investigate the magnetic and electronic properties of Co films on Fe₃O₄(001) achieved through epitaxial growth using magnetron sputtering. X-ray magnetic circularly dichroism measurements characterize the atomic magnetism. Compared to Co films on the MgO substrate, Co on Fe₃O₄ exhibits a 96% enhancement in orbital magnetic moment (from 0.25 to 0.49 μ_B/atom) and an increase in spin magnetic moment (from 1.37 to 1.53 μ_B/atom), resulting in an increased $m_{ratio}(m_l/m_s)$ from 0.18 to 0.32. This enhancement of the orbital moment emerges as a consequence of the interface interaction between Co and Fe₃O₄. Density functional theory calculations attribute this heightened orbital magnetic moment to the robust electronic exchange interactions. Our findings not only offer insights into the modulation of magnetic and electronic characteristics in Co-based magnetic heterostructures but also provide valuable implications for the potential application of magnetic oxide/ferromagnetic heterostructures in future spintronic devices.

INTRODUCTION

Manipulating the spin and orbital magnetic moments is key in applications of spintronic devices. Cobalt is a widely used magnetic material in the field of spintronics.[1] The robust magnetic properties of Co at room temperature have led to its widespread use in practical spintronic devices, especially as a highly spin-polarized spin injection and detection electrode.[2–4] There have been many reported works on the enhancement of orbital magnetic moment in Co induced by the ferromagnet (FM)/non-magnet (NM) interfaces.[5–7] Demonstrations in previous studies indicate a twofold enhancement of the orbital moment in the first layer of Co grown on a Cu(100) surface compared to the bulk.[8] Another investigation on epitaxially grown Co on Cu (001) revealed a 15% increase in spin magnetic moment, along with 96% and 53% increments in orbital magnetic moments parallel and perpendicular to the surface, respectively.[9] A separate study observed a notably enhanced perpendicular Co orbital moment in Co/Pt multilayers exhibiting perpendicular magnetic anisotropy (PMA).[10]

In recent years, there has been a growing body of research on heterostructures involving combinations of magnetic oxide and ferromagnetic layers. For example, a study demonstrated the effective elimination of spin backflow and spin-memory loss at Pt-based heavy metal–ferromagnet interfaces by inserting an insulating

27 November 2024 10:49:45

paramagnetic NiO layer of optimum thickness in the heavy metal/NiO/ferromagnetic metal structure.[11] Another investigation reported the temperature-dependent damping-like spin–orbit torque (SOT) in Pt/NiO/CoFeB, showing a reversal of sign below certain temperatures, in contrast to the slight variation with temperature observed in the Pt/CoFeB bilayer.[12] In addition, another study detailed the experimental demonstration of deterministic current-induced spin–orbit torque (SOT) switching in a magnetic heterostructure comprising Fe_2O_3/Ta/CoFeB/MgO, showcasing robust perpendicular anisotropy. The findings revealed that the Fe_2O_3 underlayer significantly reduces the critical magnetization switching current by 70% and enhances the efficiency of the SOT current-driven switching process.[13]

However, studies on the magnetic moment of ferromagnetic thin films in magnetic oxide/ferromagnetic heterostructures are still limited. Notably, magnetite (Fe_3O_4) has emerged as a particularly promising candidate due to its high-temperature stability and robust ferrimagnetism. Theoretical predictions have indicated that Fe_3O_4 exhibits a 100% spin polarization near the Fermi level (E_F).[14,15] This unique property has generated significant interest in Fe_3O_4 as a potential material for spintronics.[16,17] Therefore, demonstrating the enhancement of the orbital moment in the Co/Fe_3O_4 system contributes to a deeper understanding of the interplay between the magnetic layer and the magnetic oxide layer. The significant enhancement of the orbital moment in this system offers possibilities for tailored spin manipulation and control, which are crucial for the development of advanced spintronic devices. Specifically, we observe a nearly doubled orbital magnetic moment in Co thin films grown on Fe_3O_4, providing a new opportunity to tune the magnetic and electronic properties of Co-based spintronic devices.

EXPERIMENTAL

In this work, Co/Fe_3O_4 heterostructure thin films were epitaxially grown on MgO(001) substrates using magnetron sputtering. More specifically, a high-quality Fe_3O_4(001) thin film was grown by sputtering a pure iron target in a magnetron sputtering system, introducing a mixture of argon and oxygen gases. As shown in Fig. 1(a), the MgO substrate was annealed at 500 °C for 60 minutes under a base pressure of 1×10^{-8} Torr, and the reflection high-energy electron diffraction (RHEED) patterns revealed a remarkably smooth surface of the substrate.[18] The RHEED measurements were *in situ* performed after the growth of each layer. MgO belongs to the cubic crystal system, and the RHEED patterns of MgO(001) exhibit two distinct directions, MgO[001] and MgO[0–11]. The other directions share the same symmetry and are equivalent due to the crystal's symmetry properties. Hence, we present RHEED patterns along these two directions. Then the substrate temperature was fixed at 300 °C during the Fe_3O_4 deposition process. An RF power source was utilized, with the flow rate of oxygen controlled at 1.5 SCCM and the flow rate of argon at ~50 SCCM. Figure 1(b) shows the RHEED pattern of the 3 nm Fe_3O_4(001) film grown on a MgO(001) substrate. The image confirms a specific $\left(\sqrt{2} \times \sqrt{2}\right)R45°$ reconstruction of the Fe_3O_4(001) surface.[18,19] The sharp and distinct RHEED lines as well as the appearance of Laue oscillations in Fig. 1(b) indicate that the grown film is a single-crystal Fe_3O_4 film with a highly well-ordered and flat surface.[19,20] In consideration of the limited detection depth
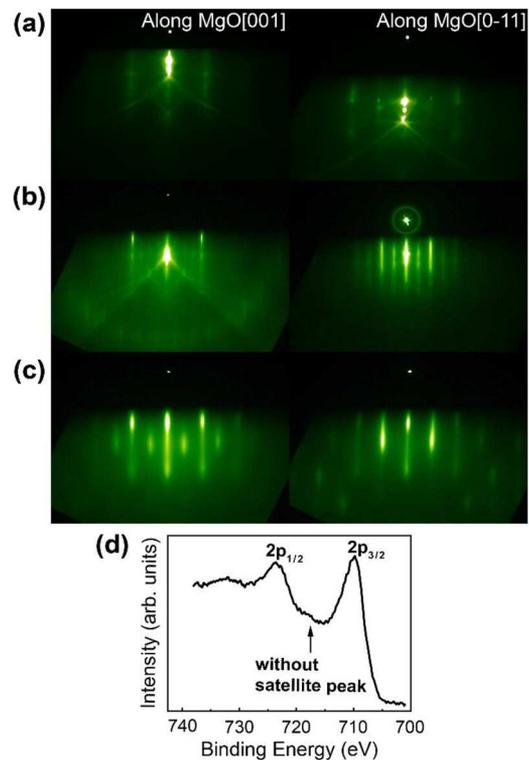

FIG. 1. Reflection high-energy electron diffraction (RHEED) patterns of the (a) MgO(001) substrate, (b) 3 nm Fe_3O_4 film, and (c) 3 nm fcc Co film. (d) Fe 2p x-ray photoemission spectroscopy (XPS) spectra of the 3 nm Fe_3O_4 film. The absence of a satellite peak confirms the nonexistence of γ-Fe_2O_3.

in x-ray magnetic circular dichroism (XMCD) testing,[21] a 3 nm epitaxial single-crystal Co thin film with an fcc structure[22] was subsequently grown on the Fe_3O_4(001) thin film by magnetron sputtering at room temperature, as shown in Fig. 1(c). Numerous studies have emphasized the feasibility and significance of achieving single-crystalline growth under notable interfacial strain conditions.[23,24] It is worth noting that the lattice constant of MgO is 4.216 Å while that of Fe_3O_4 is 8.396 Å, nearly double that of MgO. Therefore, Co grown on both substrates exhibits a similar lattice mismatch and resulting strain state. Ultimately, a 2 nm Ta capping layer was grown to protect the film from oxidation.

The Fe 2p core-level x-ray photoemission spectroscopy (XPS) spectra of the Fe_3O_4(001) film are presented in Fig. 1(d). The spectrum exhibits two distinctive Fe_3O_4 peaks at 711 and 724 eV, which correspond to the binding energies of Fe^{2+} $2p_{3/2}$ and Fe^{2+} $2p_{1/2}$, respectively.[25–27] No satellite peaks were observed, thereby excluding the possible presence of γ-Fe_2O_3.[28] The metal–insulator transition, known as Verwey transition, is a defining characteristic of Fe_3O_4 and serves as strong evidence for the high quality of the magnetite thin films that we have grown.[29] Figure S1(a) shows the resistivity as a function of temperature for the 40 nm Fe_3O_4 film, and the Verwey transition occurs around 130 K (T_V), which is consistent with that reported in other studies.[30–33]

The magnetic analysis of the grown films was *ex-situ* carried out using a vibrating sample magnetometer (VSM) and x-ray magnetic circularly dichroism (XMCD) measurements. XMCD is regarded as one of the most promising experimental techniques for determining the magnetic moments in ultrathin films.[34] The x-ray absorption (XAS) was measured at room temperature under an applied magnetic field of 4000 Oe parallel to the sample plane by total electron yield (TEY) detection.[21] The 100% circularly polarized x rays were incident at an angle of 30° with respect to the sample plane.[9,35] During testing, we employed continuous sweeps, and at each measurement point, a dwell time of 1.5 s was utilized. By utilizing the so-called sum rules, XMCD provides valuable insights into the spin and orbital magnetic moments separately, allowing for more precise evaluation.[36,37]

RESULTS AND DISCUSSION

The magnetic hysteresis loops of the 3 nm Fe_3O_4 film with an applied magnetic field along the MgO[001] and MgO[0–11] directions are shown in Fig. 2(a). The saturation magnetization (Ms) of the thin film is ~450 ± 21 emu/cm³ along the MgO[001] direction, which is slightly lower than the value of 480 emu/cm³ for bulk magnetite.[38] The magnetic hysteresis loops of the MgO/Fe_3O_4 (3 nm)/Co

(3 nm)/Ta film are shown in Figs. 2(b) and 2(c). The magnetic hysteresis loop in the M–H curve shows a consistent magnetization reversal behavior in the MgO/Fe_3O_4 (3 nm)/Co (3 nm)/Ta thin film. This indicates a well-defined magnetic anisotropy in the film and suggests a potential for its application in spintronic devices. It is worth noting that the decrease in *Ms* compared to the MgO/Co (3 nm)/Ta film is expected due to the use of the total thickness of the film in calculating the value of *Ms*.

Figure 2(d) illustrates the Fe $L_{2,3}$-edge XAS and XMCD spectra of the Fe_3O_4 in MgO/Fe_3O_4 (3 nm)/Co (3 nm)/Ta thin film. In $[Fe_{td}^{3+}]_A[Fe_{oh}^{3+} Fe_{oh}^{2+}]_BO_4$, the antiparallel spin orientations of the A and B sites give rise to distinct contributions from various sites of Fe_{td}^{3+}, Fe_{oh}^{2+}, and Fe_{oh}^{3+}, which can be distinguished.[39–45] The values of spin moment m_s and orbital moment m_l were calculated by applying sum rules on the integrated XMCD and total XAS spectra based on the following equation:[36,37]

$$m_l = -\frac{4}{3}n_h \frac{\int_{L_{2,3}} \left(\sigma^+ - \sigma^-\right)dE}{\int_{L_{2,3}} \left(\sigma^+ + \sigma^-\right)dE}$$

$$m_s + \langle T_z \rangle = -n_h \frac{6\int_{L_3} \left(\sigma^+ - \sigma^-\right)dE - 4\int_{L_{2,3}} \left(\sigma^+ - \sigma^-\right)dE}{\int_{L_{2,3}} \left(\sigma^+ + \sigma^-\right)dE},$$

(1)

where n_h is the effective number of 3d-band holes,[40] which had been taken from Refs. 9, 40, and 46. The magnetic dipole term $\langle T_Z \rangle$ is negligible because of the predominantly cubic symmetry of magnetite and cobalt even considering additional surface symmetry breaking.[8,38] The background of each XAS spectrum was fitted by an arctangent-based step function,[47] as shown in Figs. 2(d)–2(f). We obtained the values of $m_s = 2.49 \pm 0.16\ \mu_B/f$ u and $m_l = 0.29 \pm 0.05 \cdot \mu_B/f$ u, while the total moment for the 3 nm Fe_3O_4 in MgO/Fe_3O_4 (3 nm)/Co (3 nm)/Ta thin film $m_{l+s} = 2.78 \pm 0.21\ \mu_B/f$ u.

Figures 2(e) and 2(f) illustrate the Co $L_{2,3}$-edge XAS and XMCD spectra for MgO/Co (3 nm)/Ta and MgO/Fe_3O_4 (3 nm)/Co (3 nm)/Ta films, respectively. According to the shape and position of the absorption spectrum, no evidence of oxidation of the Co layer by oxygen from the underlying layer or the external environment was observed within the sensitivity range of the measurement. By comparison, the decreasing intensity of the XMCD at the L_2-edge shown in Fig. 2(f) indicates the stronger orbital magnetism.[8,35] This result is verified by the values obtained from the calculation of Eq. (1). We obtained the values of $m_s = 1.37 \pm 0.07\ \mu_B/atom$ (1.53 ± 0.08 $upmu_B/$ atom)and $m_l = 0.25 \pm 0.01\ \mu_B/atom$ (0.49 ± 0.02 μ_B/atom), while the total moment for the 3 nm Co layer in the MgO/Co/Ta (MgO/Fe_3O_4/Co/Ta) film $m_{l+s} = 1.62 \pm 0.08\ \mu_B/atom$ (2.02 ± 0.10 μ_B/atom). As demonstrated in Table SI, the value of m_l for the MgO/Co/Ta film falls within the range reported in other literature studies.[5,8–10,47,48] For example, a study on 2.1 Ml Co/Cu(001)[48] reported $m_l = 0.24 \pm 0.05\ \mu_B$/atom. Notably, this value aligns closely with the present result within the error bar. The total magnetic moment is increased by 24.7%. The spin magnetic moment increased by 11.7%. In particular, compared to the Co layer grown on the MgO substrate, the magnitude of the orbital magnetic moment of the Co layer grown on Fe_3O_4 is increased by almost a factor of two. This leads to a significant increase in $m_{ratio}(m_l/m_s)$, from 0.18 to 0.32.
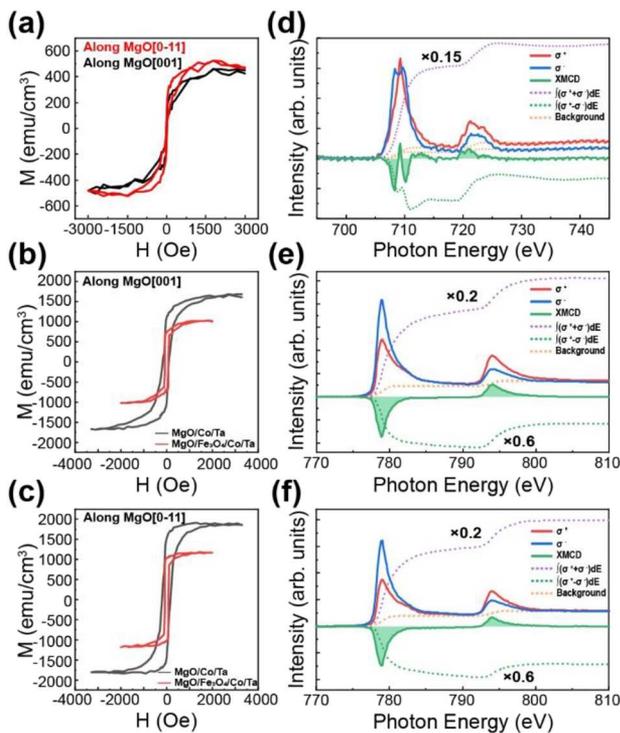

FIG. 2. Vibrating sample magnetometer (VSM) magnetization curves of the (a) 3 nm Fe_3O_4 film, (b) MgO/Co (3 nm)/Ta film, and (c) MgO/Fe_3O_4 (3 nm)/Co (3 nm)/Ta film. (d) Fe $L_{2,3}$-edge x-ray absorption (XAS) and x-ray magnetic circularly dichroism (XMCD) spectra of the Fe_3O_4 in MgO/Fe_3O_4 (3 nm)/Co (3 nm)/Ta thin film. Co $L_{2,3}$-edge XAS and XMCD spectra of the (e) MgO/Co (3 nm)/Ta film and (f) MgO/Fe_3O_4 (3 nm)/Co (3 nm)/Ta film.

To investigate the role of the Fe_3O_4/Co interface on the enhancement of the magnetic moment, especially the orbital magnetic moment, we measured the following series of samples with a thin Cr interlayer between Fe_3O_4 and Co layers: MgO/Fe_3O_4 (3 nm)/Cr (n)/Co (3 nm)/Ta (n = 0.3, 0.5, 1, 3, 5, 10 nm). The RHEED patterns for the Cr interlayer, as illustrated in Fig. S3, confirm the single-crystal epitaxial growth of the Cr layer. It can be clearly seen from Fig. 3 that when the thickness of Cr is below 1 nm, there is a significant enhancement in the m_l and m_{ratio} of the Co layer. This suggests that the absence of a continuous film when the thickness of Cr is less than 1 nm results in little effect on the coupling interaction between Co and Fe_3O_4 at the interface. At a thickness of 3 nm of Cr, m_l and m_{ratio} sharply decrease and their values are close to that of the MgO/Co (3 nm)/Ta film, indicated by the hollow shape in Fig. 3. The results confirm that the enhancement of the magnetic moment in Co originates from the interface between Co and Fe_3O_4(001).

To investigate whether this enhancement of orbital magnetism exists in Co bilayer structures with other iron oxides, we deposited Co on thin films of various iron oxides. When sputtering pure iron targets, modification of the oxygen-to-argon gas ratio in the reaction can result in thin films of iron oxide with varying compositions. During the film growth process, a 50 SCCM Ar gas flow was introduced, while the flow rate of O_2 was controlled from 0.0 to 2.0 SCCM. With an increasing O_2 flow rate, the oxidation degree of the deposited films is gradually enhanced. Previous study had demonstrated that O_2 flow rates of 1.5 and 1.7 SCCM

are suitable conditions for the growth of Fe_3O_4 thin film.[18] As shown in Fig. 4(a), the values of the magnetic moment of the 3 nm Co layer in MgO/FeO_x (3 nm)/Co (3 nm)/Ta films significantly increase at O_2 flow rates of 1.5 and 1.7 SCCM. A similarly enhanced orbital magnetic moment led to a significant increase in m_{ratio}, as shown in Fig. 4(b). At an oxygen flow rate of 2 SCCM, the formation of γ-Fe_2O_3 thin films was achieved.[18] We obtained values of m_s = 1.26 ± 0.06 μ_B/atom and m_l = 0.27 ± 0.01 μ_B/atom, while the total moment for the 3 nm Co layer in the MgO/γ-Fe_2O_3/Co/Ta film m_{l+s} = 1.53 ± 0.07 μ_B/atom. Relative to the Co layer grown on a MgO substrate, the orbital magnetic moment demonstrates an 8% enhancement, resulting in an increased m_{ratio} of 0.21. This result confirms that the interaction between Co and Fe ions in Fe_3O_4 is notably stronger than their interaction in other iron oxide counterparts.

To complement our experimental results, we performed first-principles density functional theory (DFT)[49] calculations using the Vienna *Ab initio* Simulation Package (VASP)[50] to investigate the electronic and magnetic properties of the studied materials. We used the projected augmented wave (PAW) method to describe electron–ion interactions[51] and the generalized gradient approximation (GGA) to handle the electronic exchange-correlation functional.[52] To obtain the magnitude of the orbital magnetic moments, the spin–orbit coupling was explicitly included in the Hamiltonian.[53] Therefore, our calculation method corresponds to a fully relativistic GGA + U approach. It has been demonstrated that the GGA + U method is suitable for accurately describing the orbital
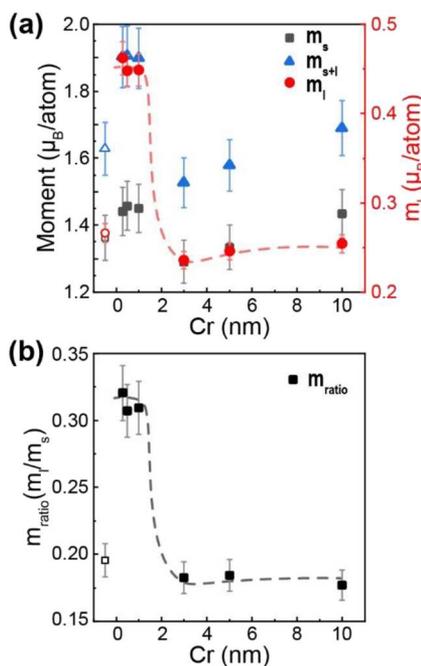
FIG. 3. (a) Magnetic moment and (b) $m_{ratio}(m_l/m_s)$ of the 3 nm Co layer in MgO/Fe_3O_4 (3 nm)/Cr (n)/Co (3 nm)/Ta (n = 0.3, 0.5, 1, 3, 5, and 10 nm) films. Hollow symbols represent the values of the MgO/Co (3 nm)/Ta film. The dashed lines are guidelines for the eye.

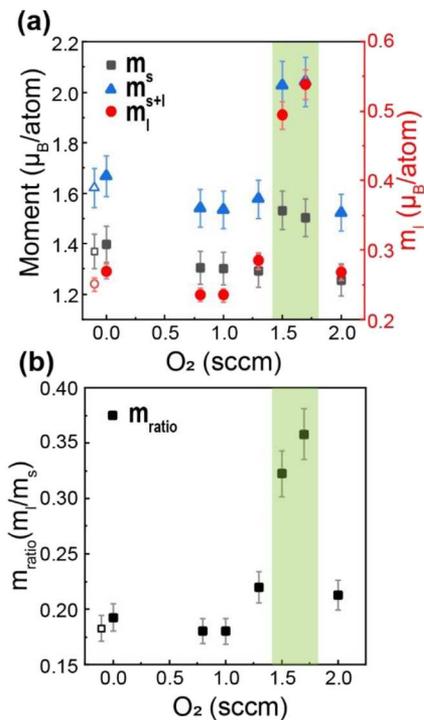**FIG. 4.** (a) Magnetic moment and (b) $m_{ratio}(m_l/m_s)$ of the 3 nm Co layer in MgO/FeO_x (3 nm)/Co (3 nm)/Ta films. Hollow symbols represent the values of the MgO/Co (3 nm)/Ta film.

magnetism of solids with strongly correlated electrons.[54] To better account for the Co 3d electrons, we utilized the GGA + U method[55] with U_{eff} = 3 eV.[56–58] The plane-wave cutoff energy was set to 400 eV, and the structural relaxation forces were constrained to below 0.01 eV/Å per atom. Additional details on the DFT calculations are provided in the supplementary material.

The GGA + U structural model of fcc Co on the Fe_3O_4(001) surface is shown in Fig. 5(a). Fe_3O_4 has a cubic inverse spinel structure AB_2O_4, in which the larger oxygen anions form a face-centered-cubic structure. In the O^{2-} lattice, only Fe^{3+} ions occupy the tetrahedral (A) sites, and Fe^{2+}/Fe^{3+} ions occupy the octahedral (B) sites. The magnetic moments corresponding to the density of states (DOS) shown in Figs. 5(b) and 5(c) are 1.850 μ_B/atom and 2.116 μ_B/atom for 3 nm Co on MgO and 3 nm Co on Fe_3O_4, respectively. The corresponding values for the spin moment are 1.652 and 1.814 μ_B/atom, and the corresponding values for the orbital moment are 0.198 and 0.302 μ_B/atom, respectively. The total magnetic moment for the fcc Co on Fe_3O_4 is increased by 14.4%. The spin magnetic moment increased by 9.8%. It is worth noting that, consistent with the experimental results, the increase in orbital magnetic moment is more significant, with a 52.5% increase. This leads to an increase in m_{ratio} from 0.12 to 0.17. To validate the accuracy of the calculation results, the magnetic moments of Co on the Fe_3O_4
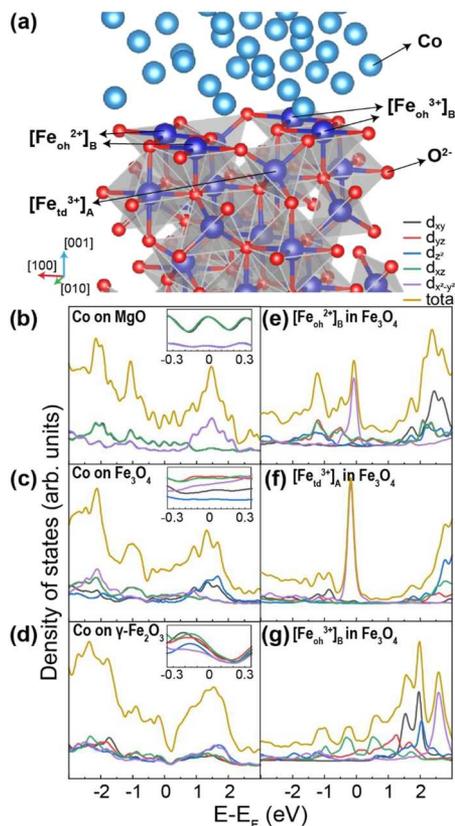
TABLE I. The magnetic moments (μ_B) for the Co films calculated by the GGA + U method with different U_{eff} values.

U_{eff}	MgO/Co (3 nm)			MgO/Fe_3O_4(001) (3 nm)/Co (3 nm)		
	m_l	m_s	$m_l + m_s$	m_l	m_s	$m_l + m_s$
0	0.076	1.564	1.640	0.090	1.840	1.930
2	0.141	1.708	1.849	0.175	1.816	1.991
2.5	0.147	1.704	1.851	0.186	1.698	1.884
3	0.198	1.652	1.850	0.302	1.814	2.116
3.5	0.231	1.622	1.853	0.320	1.735	2.055

were calculated using the GGA + U method with different U_{eff} values (0, 2, 2.5, 3, and 3.5), and the results are presented in Table I, which show an increase in the magnetic moment of the Co layer on Fe_3O_4 for different U values.

In Figs. 5(b)–5(g), the density of states (DOS) based on GGA + U calculations are presented. The DOS of Fe ions in Fe_3O_4 near the Co/Fe_3O_4 interface is illustrated in Figs. 5(e)–5(g), revealing a distinct peak near the Fermi level for $[Fe_{oh}^{2+}]_B$ and $[Fe_{td}^{3+}]_A$ ions. This is attributed to Fe_3O_4 acting as a semi-metallic material, where electron states near the Fermi level are occupied, resulting in an increase in the electronic density of states.[59] The localization of electron states for Fe ions results in a robust electronic exchange interaction between Co and Fe_3O_4. The increased hybridization between Fe ions and Co atoms substantially influences the electronic states of Co, leading to the splitting of the energy levels of Co's 3d orbital electrons, as shown in Fig. 5(c). This splitting arises from electron–electron interactions, constituting a prevalent electronic structural effect.[60,61] Conventionally, removing the degeneracy from the d-orbital manifold quenches the orbital moment. However, an enhanced orbital magnetic moment is observed for the Co layer grown on Fe_3O_4, which is also attributed to the strong electronic exchange interactions between Co and Fe_3O_4. This process is governed by the complex interplay between electron spin and orbital motion, which is crucial in determining the orbital magnetic moment. The localization of $[Fe_{oh}^{2+}]_B$ and $[Fe_{td}^{3+}]_A$ ions is a pivotal factor influencing the electronic exchange interactions. DFT calculations for the Co/γ-Fe_2O_3 structure provide corroborative evidence for these findings. The magnetic moment for 3 nm Co on γ-Fe_2O_3 is 2.030 μ_B/atom, corresponding to the DOS shown in Fig. 5(d). The corresponding values for the spin moment and orbital moment are 1.780 and 0.250 μ_B/atom. The orbital magnetic moment has been increased compared to the theoretical value for Co on MgO, and this enhancement is reduced by half compared to that observed for Co on Fe_3O_4. This phenomenon arises from the molecular expression of γ-Fe_2O_3 as $[Fe_{td}^{3+}]_A[Fe_{oh}^{3+}_{5/3}※_{1/3}]_BO_4$ (※indicating a vacancy). With the same crystal lattice structure as Fe_3O_4, γ-Fe_2O_3 undergoes a transition where 2/3 of $[Fe_{oh}^{2+}]_B$ positions convert to Fe^{3+} ions, while 1/3 of the positions become vacancies. This alteration is anticipated to lead to a diminished electronic exchange interaction with the Co layer, subsequently weakening its impact on the orbital magnetic moment.

CONCLUSION

In summary, we have investigated the magnetic and electronic properties of Co films grown on Fe_3O_4(001). The epitaxial growth of

FIG. 5. (a) GGA + U structural model of fcc Co on the Fe_3O_4(001) surface. Density of states (DOS) for (b) Co on MgO, (c) Co on Fe_3O_4, (d) Co on γ-Fe_2O_3, (e) $[Fe_{oh}^{2+}]_B$ ions, (f) $[Fe_{td}^{3+}]_A$ ions, and (g) $[Fe_{oh}^{3+}]_B$ ions in Fe_3O_4.

a single-crystalline fcc-structured Co film on the Fe_3O_4(001) surface has been achieved. We employed XMCD measurements to characterize the atomic magnetism of the thin film. The results showed that compared to the Co thin film grown on the MgO substrate, the orbital magnetic moment of Co on the Fe_3O_4 surface increased from 0.25 ± 0.01 to 0.49 ± 0.02 μ_B/atom, showing a 96% enhancement. The relative enhancement of the orbital moment is thus very large, much larger than the enhancement of the spin moment. This leads to a significant increase in $m_{ratio}(m_l/m_s)$, increasing from 0.18 to 0.32. Then we determined that this enhancement originates from the interface interaction between Co and Fe_3O_4 by inserting a Cr interlayer between them. The DFT calculations reveal that the exchange interaction between the Co and Fe ions, particularly involving $[Fe_{oh}^{2+}]_B$ and $[Fe_{td}^{3+}]_A$ ions, profoundly impacts Co's electronic states. This, in turn, contributes to the enhancement of Co's orbital magnetic moment. Furthermore, the interaction between Co and Fe ions in Fe_3O_4 is notably stronger than their interaction in other iron oxide counterparts. The presence of unquenched m_l, or strong spin–orbit coupling, is highly desirable in terms of controllability through an electric field in spintronics operations. By enhancing the orbital moment, we can obtain higher Magnetic Anisotropy Energy(MAE). A large MAE creates a potential well that protects the system's magnetization in a specific direction, ensuring long-term stability against thermal disturbances. This, consequently, facilitates the stable storage of information at the atomic scale.[62] Moreover, the enhanced orbital moment provides valuable insights into the potential applications of magnetic oxide/ferromagnetic heterostructures in future spintronic devices, leading to improved performance. It opens up opportunities for developing efficient spin manipulation techniques, enhancing device functionality, and realizing novel spin-based functionalities.

SUPPLEMENTARY MATERIAL

See the supplementary material for the Verwey transition of Fe_3O_4, analysis of RHEED patterns for the samples, XAS and XMCD spectra of the samples, and details on the DFT calculations.

AUTHOR DECLARATIONS

Conflict of Interest

The authors have no conflicts to disclose.

Author Contributions

Zhe Zhang: Conceptualization (equal); Data curation (lead); Formal analysis (lead); Investigation (lead); Methodology (lead); Project administration (lead); Software (equal); Validation (equal); Visualization (equal); Writing – original draft (lead). **Xianyang Lu**: Conceptualization (equal); Funding acquisition (lead); Investigation (equal); Methodology (equal); Project administration (lead); Resources (lead); Supervision (equal); Writing – review & editing (lead). **Zhihao Li**: Data curation (equal); Methodology (equal); Software (equal). **Zhuoyi Li**: Formal analysis (equal); Validation (equal); **Yu Yan**: Funding acquisition (equal). Yuzhe Chen: Investigation (equal). Jun Du: Methodology (equal); Resources (equal). Fangyuan Zhu: Methodology (equal). **Jiefeng Cao**: Methodology (equal). Yong Wang: Methodology (equal). **Yao Li**: Funding acquisition (equal); Resources (equal); Supervision (equal). Liang He: Funding acquisition (equal); Resources (equal); Validation (equal). **Jing Wu**: Supervision (equal); Validation (equal). **Rong Zhang**: Resources (equal). **Yongbing Xu**: Conceptualization (lead); Funding acquisition (equal); Investigation (equal); Project administration (equal); Resources (equal); Supervision (lead); Validation (equal); Writing – review & editing (lead).

DATA AVAILABILITY

The data that support the findings of this study are available from the corresponding authors upon reasonable request.

REFERENCES

[1] W. Liu, P. K. J. Wong, and Y. Xu, Prog. Mater. Sci. **99**, 27 (2019).
[2] F. J. Jedema, H. B. Heersche, A. T. Filip, J. J. Baselmans, and B. J. van Wees, Nature **416**, 713 (2002).
[3] S. Takahashi and S. Maekawa, Phys. Rev. B **67**, 052409 (2003).
[4] F. J. Jedema, M. S. Nijboer, A. T. Filip, and B. J. van Wees, Phys. Rev. B **67**, 085319 (2003).
[5] P. Ryan, R. P. Winarski, D. J. Keavney, J. W. Freeland, R. A. Rosenberg, S. Park, and C. M. Falco, Phys. Rev. B **69**, 054416 (2004).
[6] P. Gambardella, A. Dallmeyer, K. Maiti, M. C. Malagoli, W. Eberhardt, K. Kern, and C. Carbone, Nature **416**, 301 (2002).
[7] H. A. Dürr, G. van der Laan, J. Vogel, G. Panaccione, N. B. Brookes, E. Dudzik, and R. McGrath, Phys. Rev. B **58**, R11853 (1998).
[8] M. Tischer, O. Hjortstam, D. Arvanitis, J. Hunter Dunn, F. May, K. Baberschke, J. Trygg, J. M. Wills, B. Johansson, and O. Eriksson, Phys. Rev. Lett. **75**, 1602 (1995).
[9] T. Nakagawa, Y. Takagi, Y. Matsumoto, and T. Yokoyama, Jpn. J. Appl. Phys. **47**, 2132 (2008).
[10] N. Nakajima, T. Koide, T. Shidara, H. Miyauchi, H. Fukutani, A. Fujimori, K. Iio, T. Katayama, M. Nývlt, and Y. Suzuki, Phys. Rev. Lett. **81**, 5229 (1998).
[11] L. Zhu, L. Zhu, and R. A. Buhrman, Phys. Rev. Lett. **126**, 107204 (2021).
[12] D. Zhu, T. Zhang, X. Fu, R. Hao, A. Hamzic, H. Yang, X. Zhang, H. Zhang, A. Du, D. Xiong, K. Shi, S. Yan, S. Zhang, A. Fert, and W. Zhao, Phys. Rev. Lett. **128**, 217702 (2022).
[13] Z. Li, X. Lu, Z. Zhang, W. Li, T. T. Li, J. Zhou, Y. Yan, R. Liu, J. Du, R. Liu, X. Wang, Y. Li, L. He, J. Wu, R. Zhang, and Y. Xu, Appl. Phys. Lett. **123**, 042404 (2023).
[14] Z. Zhang and S. Satpathy, Phys. Rev. B **44**, 13319 (1991).
[15] Y. S. Dedkov, U. Rüdiger, and G. Güntherodt, Phys. Rev. B **65**, 064417 (2002).
[16] M. Bibes, J. E. Villegas, and A. Barthélémy, "Ultrathin oxide films and interfaces for electronics and spintronics," Adv. Phys. **60**, 5 (2011).
[17] S. G. Bhat and P. S. Anil Kumar, AIP Adv. **6**, 056308 (2016).
[18] Z. Zhang, X. Lu, Y. Yan, J. Lu, Z. Li, Q. Liu, F. Zhu, J. Cao, Y. Wang, Z. Huang, Y. Zhai, Y. Li, X. Ruan, L. He, J. Wu, J. Du, R. Zhang, and Y. Xu, Appl. Phys. Lett. **120**, 182403 (2022).
[19] D. J. Huang, C. F. Chang, J. Chen, L. H. Tjeng, A. D. Rata, W. P. Wu, S. C. Chung, H. J. Lin, T. Hibma, and C. T. Chen, J. Magn. Magn. Mater. **239**, 261 (2002).

[20] T. Fujii, M. Takano, R. Katano, Y. Isozumi, and Y. Bando, J. Magn. Magn. Mater. **130**, 267 (1994).

[21] M. Kasrai, W. N. Lennard, R. W. Brunner, G. M. Bancroft, J. A. Bardwell, and K. H. Tan, Appl. Surf. Sci. **99**, 303 (1996).

[22] M. Ohtake, O. Yabuhara, J. Higuchi, and M. Futamoto, J. Appl. Phys. **109**, 07C105 (2011).

[23] N. Itagaki, Y. Nakamura, R. Narishige, K. Takeda, K. Kamataki, K. Koga, M. Hori, and M. Shiratani, Sci. Rep. **10**, 4669 (2020).

[24] Y. Nakamura, N. Yamashita, K. Kamataki, T. Okumura, K. Koga, M. Shiratani, and N. Itagaki, Cryst. Growth Des. **22**, 3770 (2022).

[25] D. Wilson and M. A. Langell, Appl. Surf. Sci. **303**, 6 (2014).

[26] T. Yamashita and P. Hayes, J. Electron Spectrosc. Relat. Phenom. **152**, 6 (2006).

[27] Y. Gao and S. A. Chambers, J. Cryst. Growth **174**, 446 (1997).

[28] Y. X. Lu, J. S. Claydon, E. Ahmad, Y. B. Xu, M. Ali, B. J. Hickey, S. M. Thompson, J. A. D. Matthew, and K. Wilson, J. Appl. Phys. **97**, 10C313 (2005).

[29] M. S. Senn, J. P. Wright, and J. P. Attfield, Nature **481**, 173 (2011).

[30] M. Bohra, N. Agarwal, and V. Singh, J. Nanomater. **2019**, 8457383.

[31] M. Taguchi, A. Chainani, S. Ueda, M. Matsunami, Y. Ishida, R. Eguchi, S. Tsuda, Y. Takata, M. Yabashi, K. Tamasaku, Y. Nishino, T. Ishikawa, H. Daimon, S. Todo, H. Tanaka, M. Oura, Y. Senba, H. Ohashi, and S. Shin, Phys. Rev. Lett. **115**, 256405 (2015).

[32] H. T. Jeng, G. Y. Guo, and D. J. Huang, Phys. Rev. Lett. **93**, 156403 (2004).

[33] X. Liu, C.-F. Chang, A. D. Rata, A. C. Komarek, and L. H. Tjeng, npj Quantum Mater. **1**, 16027 (2016).

[34] C. T. Chen, F. Sette, Y. Ma, and S. Modesti, Phys. Rev. B **42**, 7262 (1990).

[35] P. Gambardella, S. Rusponi, M. Veronese, S. S. Dhesi, C. Grazioli, A. Dallmeyer, I. Cabria, R. Zeller, P. H. Dederichs, K. Kern, C. Carbone, and H. Brune, Science **300**, 1130 (2003).

[36] P. Carra, B. T. Thole, M. Altarelli, and X. Wang, Phys. Rev. Lett. **70**, 694 (1993).

[37] B. T. Thole, P. Carra, F. Sette, and G. van der Laan, Phys. Rev. Lett. **68**, 1943 (1992).

[38] W. Q. Liu, Y. B. Xu, P. K. J. Wong, N. J. Maltby, S. P. Li, X. F. Wang, J. Du, B. You, J. Wu, P. Bencok, and R. Zhang, Appl. Phys. Lett. **104**, 142407 (2014).

[39] M. H. Hamed, R. A. Hinz, P. Lomker, M. Wilhelm, A. Gloskovskii, P. Bencok, C. Schmitz-Antoniak, H. Elnaggar, C. M. Schneider, and M. Muller, ACS Appl. Mater. Interfaces **11**, 7576 (2019).

[40] D. J. Huang, C. F. Chang, H. T. Jeng, G. Y. Guo, H. J. Lin, W. B. Wu, H. C. Ku, A. Fujimori, Y. Takahashi, and C. T. Chen, Phys. Rev. Lett. **93**, 077204 (2004).

[41] C. Love, J. E. Beevers, B. Achinuq, R. Fan, K. Matsuzaki, T. Susaki, V. K. Lazarov, S. S. Dhesi, G. van der Laan, and S. A. Cavill, Phys. Rev. B **107**, 064414 (2023).

[42] R. Moreno, S. Poyser, D. Meilak, A. Meo, S. Jenkins, V. K. Lazarov, G. Vallejo-Fernandez, S. Majetich, and R. F. L. Evans, Sci. Rep. **10**, 2722 (2020).

[43] S. D. Oberdick, A. Abdelgawad, C. Moya, S. Mesbahi-Vasey, D. Kepaptsoglou, V. K. Lazarov, R. F. L. Evans, D. Meilak, E. Skoropata, J. van Lierop, I. Hunt-Isaak, H. Pan, Y. Ijiri, K. L. Krycka, J. A. Borchers, and S. A. Majetich, Sci. Rep. **8**, 3425 (2018).

[44] K. P. McKenna, F. Hofer, D. Gilks, V. K. Lazarov, C. Chen, Z. Wang, and Y. Ikuhara, Nat. Commun. **5**, 5740 (2014).

[45] X. Lu, G. Li, Y. Gong, X. Ruan, Y. Yan, Y. Li, L. He, J. Du, V. K. Lazarov, J. Wu, R. Zhang, and Y. Xu, Appl. Surf. Sci. **572**, 151456 (2022).

[46] O. Hjortstam, J. Trygg, J. M. Wills, B. Johansson, and O. Eriksson, Phys. Rev. B **53**, 9204 (1996).

[47] C. T. Chen, Y. U. Idzerda, H. Lin, N. V. Smith, G. Meigs, E. Chaban, G. H. Ho, E. Pellegrin, and F. Sette, Phys. Rev. Lett. **75**, 152 (1995).

[48] P. Srivastava, F. Wilhelm, A. Ney, M. Farle, H. Wende, N. Haack, G. Ceballos, and K. Baberschke, Phys. Rev. B **58**, 5701 (1998).

[49] W. Kohn and L. J. Sham, Phys. Rev. **140**, A1133 (1965).

[50] G. Kresse, J. Non-Cryst. Solids **192–193**, 222 (1995).

[51] D. Hobbs, G. Kresse, and J. Hafner, Phys. Rev. B **62**, 11556 (2000).

[52] J. P. Perdew, J. A. Chevary, S. H. Vosko, K. A. Jackson, M. R. Pederson, D. J. Singh, and C. Fiolhais, Phys. Rev. B **46**, 6671 (1992).

[53] B. I. Min and Y. R. Jang, J. Phys.: Condens.Matter **3**, 5131 (1991).

[54] I. V. Solovyev, A. I. Liechtenstein, and K. Terakura, Phys. Rev. Lett. **80**, 5758 (1998).

[55] V. V. Anisimov, J. Zaanen, and O. K. Andersen, Phys. Rev. B **44**, 943 (1991).

[56] L. Wang, T. Maxisch, and G. Ceder, Phys. Rev. B **73**, 195107 (2006).

[57] C. Le, S. Qin, and J. Hu, Sci. Bull. **62**, 563 (2017).

[58] Z. Shao, J. Liang, Q. Cui, M. Chshiev, A. Fert, T. Zhou, and H. Yang, Phys. Rev. B **105**, 174404 (2022).

[59] R. Masrour, E. K. Hlil, M. Hamedoun, A. Benyoussef, O. Mounkachi, and H. El Moussaoui, J. Magn. Magn. Mater. **378**, 37 (2015).

[60] S. K. Kwon and B. I. Min, Phys. Rev. Lett. **84**, 3970 (2000).

[61] S. H. Hoseyni, K. Rahimi, B. Barakati, A. Sadeghi, and S. M. Mohseni, Physica E **128**, 114620 (2021).

[62] X. Ou, H. Wang, F. Fan, Z. Li, and H. Wu, Phys. Rev. Lett. **115**, 257201 (2015).